

# Application of a Pore Fraction Hot Tearing Model to Directionally Solidified and Direct Chill Cast Aluminum Alloys



RUIFENG DOU and A.B. PHILLION

Hot tearing susceptibility is commonly assessed using a pressure drop equation in the mushy zone that includes the effects of both tensile deformation perpendicular to the thermal gradient as well as shrinkage feeding. In this study, a Pore Fraction hot tearing model, recently developed by Monroe and Beckermann (JOM 66:1439–1445, 2014), is extended to additionally include the effect of strain rate parallel to the thermal gradient. The deformation and shrinkage pore fractions are obtained on the basis of the dimensionless Niyama criterion and a scaling variable method. First, the model is applied to the binary Al-Cu system under conditions of directional solidification. It is shown that for the same Niyama criterion, a decrease in the cooling rate increases both the deformation and shrinkage pore fractions because of an increase in the time spent in the brittle temperature region. Second, the model is applied to the industrial aluminum alloy AA5182 as part of a finite element simulation of the Direct Chill (DC) casting process. It is shown that an increase in the casting speed during DC casting increases the deformation and shrinkage pore fractions, causing the maximum point of pore fraction to move towards the base of the casting. These results demonstrate that including the strain rate parallel to the thermal gradient significantly improves the predictive quality of hot tearing criteria based on the pressure drop equation.

DOI: 10.1007/s11661-016-3590-8

© The Minerals, Metals & Materials Society and ASM International 2016

## I. INTRODUCTION

THE direct chill (DC) casting process often involves defects such as hot tearing,<sup>[1,2]</sup> cold cracks,<sup>[3–5]</sup> butt curl,<sup>[6]</sup> macro/micro segregation,<sup>[7,8]</sup> and shrinkage porosity.<sup>[9]</sup> Hot tearing and shrinkage porosity in particular have been widely recognized in the literature for more than ten decades. Shrinkage porosity is caused by the volume change occurring during solidification combined with the restricted feeding of liquid to the final solidifying region. Hot tearing is a defect with similar formation mechanisms, but additionally requires tensile deformation of the mushy zone.<sup>[10]</sup> Hot tearing and porosity are known to be inter-related. For example, it has been shown that hot tears nucleate on small intergranular pores<sup>[11]</sup> and that a reduction in porosity significantly increases semi-solid ductility.<sup>[12]</sup>

Several hot tearing criteria have been developed on the basis of different parameters, *e.g.*, strain,<sup>[13]</sup> strain rate,<sup>[14,15]</sup> alloy composition, and solidification conditions.<sup>[1,16]</sup> The so-called RDG criterion<sup>[15]</sup> is a prominent

criterion based on the liquid pressure drop in the mushy zone that combines the effects of both tensile deformation perpendicular to the thermal gradient and shrinkage feeding on hot tear formation. The hot tearing predictor is given by the strain rate that satisfies the critical pressure drop  $\Delta P_{cr}$  required for hot tear formation. Although this criterion has achieved much recognition in the literature, it cannot distinguish between shrinkage porosity and hot tearing, especially for low thermal gradients.<sup>[17]</sup>

The Niyama criterion,  $N_y$ , is commonly used as a qualitative predictor of solidification shrinkage porosity during metal casting processes.<sup>[18]</sup> Recently, Carlson and Beckermann<sup>[9]</sup> proposed a dimensionless form of the Niyama criterion,  $N_y^*$ , that directly predicts shrinkage pore fractions. As with the RDG criterion,  $N_y^*$  was developed based on the liquid pressure drop in the mushy zone, but, however, it neglects tensile deformation. Within the framework of  $N_y^*$ ,  $\Delta P_{cr}$  marks the point at which liquid flow ceases in the mushy zone. Thus, any solidification occurring after liquid feeding has ceased can result in shrinkage porosity. Monroe and Beckermann<sup>[17]</sup> later modified  $N_y^*$  by adding a term related to strain rate perpendicular to the thermal gradient into the pressure drop equation. With the same method, *i.e.*, tracking of solidification and deformation after liquid feeding cessation, both the shrinkage and deformation pore fractions were predicted. The deformation pore fraction is critical for hot tearing because this defect is related to mushy zone stresses and strains.<sup>[10]</sup> The main difference between the RDG

RUIFENG DOU, Lecturer, is with the School of Mechanical Engineering, University of Science and Technology Beijing, Beijing, 100083 China. A.B. PHILLION, formerly Associate Professor with the School of Engineering, The University of British Columbia, Kelowna, BC, V1V 1V7, Canada, is now Associate Professor with the Department of Materials Science and Engineering, McMaster University, Hamilton ON, L8S 4L7, Canada. Contact e-mail: andre.phillion@mcmaster.ca

Manuscript submitted September 7, 2015.

Article published online June 8, 2016

criterion and the work of Monroe and Beckerman is that while the former predicts a strain rate satisfying  $\Delta P_{cr}$ , the latter predicts the evolution of deformation-related porosity after  $\Delta P_{cr}$  is reached based on an given strain rate.

In this study, a Pore Fraction hot tearing model for predicting the evolution of pore fraction during solidification is presented that follows the method developed by Monroe and Beckermann<sup>[17]</sup> but additionally considers the effects of deformation parallel with the thermal gradient in the mushy zone. This model is then applied to the DC casting of an Al-Mg alloy, AA5182. The effect of casting speed on hot tear formation is investigated.

## II. MODEL DEVELOPMENT

### A. Pore Fraction Hot Tearing Model

The Niyama criterion<sup>[18]</sup> is defined as

$$Ny = \frac{G}{\sqrt{\dot{T}}}, \quad [1]$$

where  $G$  is the temperature gradient and  $\dot{T}$  is the cooling rate having a positive value if the temperature is decreasing. This criterion is evaluated at a temperature near the end of solidification, when solidification shrinkage forms.

The dimensionless Niyama criterion<sup>[9]</sup> is a modified form of Eq. [1] that allows for prediction of pore fractions during casting,

$$Ny^* = \sqrt{\frac{\Delta P_{cr} \lambda_2^2 G}{\beta \mu \Delta T_f \sqrt{\dot{T}}}}, \quad [2]$$

where  $\Delta P_{cr}$  corresponds to the critical pressure drop,  $\lambda_2$  is the secondary dendrite arm spacing (SDAS),  $\beta$  is the solidification shrinkage,  $\mu$  is the viscosity, and  $\Delta T_f = T_{liq} - T_{sol}$  is the solidification interval where  $T_{liq}$  is the liquidus temperature and  $T_{sol}$  is the temperature at which the alloy is fully solidified.

The governing equations for  $Ny^*$  consist of mass conservation using a control volume containing dendrite arms and interdendritic liquid<sup>[15]</sup> and Darcy's Law governing pressure drop in the mushy zone,

$$\text{div} \langle \rho V \rangle - V_T \frac{\partial \langle \rho \rangle}{\partial x} = 0, \quad [3]$$

$$f_l V_{lx} = -\frac{K dp}{\mu dx}, \quad [4]$$

where the notation  $\langle \cdot \rangle$  is employed to indicate values that are locally averaged over the liquid and solid phases,  $\rho$  represents density,  $V$  represents velocity,  $V_T = \frac{\dot{T}}{G}$  is the isotherm speed (growth interface velocity), with a direction aligned with that of the temperature gradient,  $\mu$  is the viscosity,  $K$  is the permeability, and  $P$  is the melt pressure. Thus, the average specific mass and

average mass flow are given by  $\langle \rho \rangle = \rho_s f_s + \rho_l f_l$ , and  $\langle \rho V \rangle = \rho_s f_s V_s + \rho_l f_l V_l$ , where  $f_l$  and  $f_s$  are the volume fractions of liquid and solid,  $f_l$  is equal to  $(1 - f_s)$ , and the densities of the two phases,  $\rho_s$  and  $\rho_l$ , are assumed to be constant but not equal.<sup>[15]</sup>

Both Monroe and Beckerman's extension of Ny\*<sup>[17]</sup> and the RDG criterion<sup>[15]</sup> were developed from Eqs. [3] and [4] based on the assumptions that: (1) fluid moves only along the thermal gradient and thus equates to a one-dimensional fluid flow, and (2) the solid deforms only in a direction transverse to the fluid motion/thermal gradient. During metal casting, the first assumption is appropriate, since the mushy zone consists of a continuous path between the liquid and solid phases enabling flow in a single direction. However, deformation of solid in a direction parallel to the thermal gradient is also possible in addition to deformation in the transverse direction. Furthermore, the amount of such deformation can be easily calculated using finite element models of casting processes (e.g., References 13,19,20).

Including the solid deformation in a direction parallel to the thermal gradient will not make the derivation of the pressure drop equation any more complex as compared to previous work. From Eq. [3], mass conservation can be presented considering solid deformation in directions both parallel and perpendicular to the thermal gradient. First, under the given assumptions, Eq. [3] can be expanded,

$$\begin{aligned} \frac{\partial(\rho_l f_l V_{lx})}{\partial x} + \frac{\partial(\rho_s f_s V_{sx})}{\partial x} + \frac{\partial(\rho_s f_s V_{sy})}{\partial y} \\ = V_T \left[ \frac{\partial(\rho_s f_s)}{\partial x} + \frac{\partial(\rho_l f_l)}{\partial x} \right], \end{aligned} \quad [5]$$

where  $V_{sx}$  and  $V_{sy}$  are the relevant solid deformation velocities as shown in Figure 1. Second, assuming that  $f_s$  and  $f_l$  only change over  $x$  (along the thermal gradient), Eq. [5] can be rewritten as

$$\frac{\partial(f_l V_{lx})}{\partial x} + (1 + \beta) \left[ V_{sx} \frac{df_s}{dx} + f_s \dot{\epsilon}_{px} + f_s \dot{\epsilon}_{py} \right] = V_T \beta \frac{\partial f_s}{\partial x}, \quad [6]$$

where  $\dot{\epsilon}_{px} = \frac{\partial V_{sx}}{\partial x}$  and  $\dot{\epsilon}_{py} = \frac{\partial V_{sy}}{\partial y}$  are the strain rates parallel with and perpendicular to the thermal gradient. Third, employing the same method as used by Rappaz *et al.*,<sup>[15]</sup> Eq. [6] can be integrated over  $x$ , giving,

$$\begin{aligned} f_l V_{lx} + (1 + \beta) \left[ V_{sx} f_s + \int f_s (\dot{\epsilon}_{px} + \dot{\epsilon}_{py}) dx \right] \\ - V_T \beta f_s = C = -V_T \beta, \end{aligned} \quad [7]$$

where the constant of integration,  $C$ , has been replaced by the boundary condition,  $C = -V_T \beta$ . This equation predicts the liquid velocity at any position in the mushy zone. Finally, Darcy's law is used to link the liquid melt pressure and velocity. Replacing the  $f_l V_{lx}$  term of Eq. [7] with Eq. [4] and then integrating from  $x_{fl} = x_{cr}$  to  $x_{fl} = 1$  gives a modified form of the pressure drop equation,

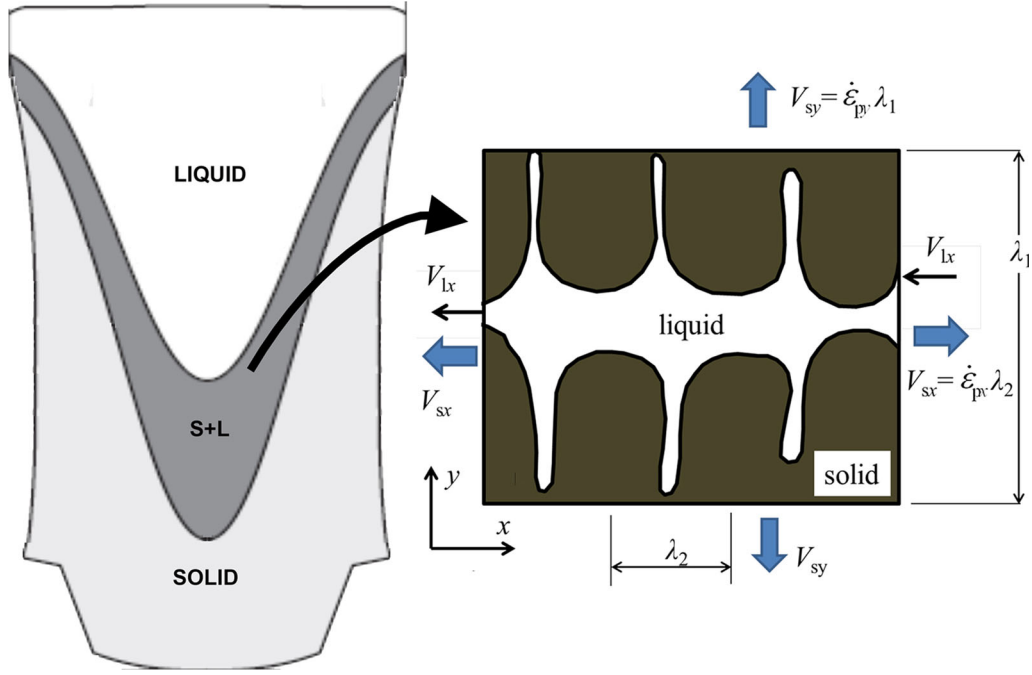


Fig. 1—Schematic of a DC cast billet showing the location of the mushy zone upon of interest in this work, along with the semi-solid microstructure (after Rappaz *et al.*<sup>[15]</sup>) upon which the mass balance is performed. Solid deformation occurs in the directions of the  $x$ - and  $y$ -axes, as indicated.

$$\Delta P_{cr} = (1 + \beta)\mu \int_{x_{f_1}=f_{cr}}^{x_{f_1}=1.0} \frac{1}{K} \left[ V_{sx} f_s + \int f_s (\dot{\epsilon}_{px} + \dot{\epsilon}_{py}) dx \right] dx + V_T \beta \mu \int_{x_{f_1}=f_{cr}}^{x_{f_1}=1.0} \frac{f_1}{K} dx \quad [8]$$

assuming that  $\mu$  and  $V_T$  are constant throughout the mushy zone. Further,  $V_T = \frac{\dot{T}}{G}$  is evaluated at a critical temperature near the solidus as defined for Ny. In this equation,  $\Delta P_{cr}$  corresponds to the critical pressure drop between  $f_1 = 1.0$  and a critical liquid fraction where feeding has ceased,  $f_{1cr}$ .

Since the temperature gradient, cooling rate, and strain rate are assumed constant, the integration variable of Eq. [8] can be changed from position to fraction liquid and the strain rate terms can be taken out of the integral, yielding,

$$\Delta P_{cr} = \frac{(1 + \beta)\mu}{G} \int_{f_{1cr}}^1 \frac{1}{K} \left[ V_{sx} f_s + \frac{(\dot{\epsilon}_{px} + \dot{\epsilon}_{py})}{G} \int_0^{f_{1cr}} (1 - f_1) \frac{dT}{df_1} df_1 \right] \frac{dT}{df_1} df_1 + \frac{\dot{T}\beta\mu}{G^2} \int_{f_{1cr}}^1 \frac{f_1}{K} \frac{dT}{df_1} df_1 \quad [9]$$

If the strain rates ( $\dot{\epsilon}_{px}$  and  $\dot{\epsilon}_{py}$ ) are set to zero, Eq. [9] is identical with the result of Carlson and Beckerman<sup>[9]</sup> in deriving Ny\* since the term  $V_{sx} f_s = 0$

(recall that  $\dot{\epsilon}_{px} = \frac{\partial V_{sx}}{\partial x}$  by definition) and can be used for predicting shrinkage porosity. If only  $\dot{\epsilon}_{px}$  is set to zero, Eq. [12] matches the RDG criterion<sup>[15]</sup>

Introducing a dimensionless temperature,  $\theta = (T - T_{sol})/\Delta T_f$  where  $\Delta T_f$  is the freezing range of the alloy and rearranging Eq. [9] yields

$$\Delta P_{cr} = \frac{(1 + \beta)\mu\Delta T_f^2 (\dot{\epsilon}_{px} + \dot{\epsilon}_{py})}{G^2} I_{de} + \frac{(1 + \beta)\mu\Delta T_f \dot{\epsilon}_{px} \lambda_2}{G} I_{sh\dot{\epsilon}} + \frac{\dot{T}\beta\mu\Delta T_f}{G^2} I_{sh}, \quad [10a]$$

$$I_{de} = \int_{f_{1cr}}^1 \left[ \frac{1}{K} \int_0^{f_{1cr}} (1 - f_1) \frac{d\theta}{df_1} df_1 \right] \frac{d\theta}{df_1} df_1, \quad [10b]$$

$$I_{sh\dot{\epsilon}} = \int_{f_{1cr}}^1 \frac{1 - f_1}{K} \frac{d\theta}{df_1} df_1, \quad [10c]$$

$$I_{sh} = \int_{f_{1cr}}^1 \frac{f_1}{K} \frac{d\theta}{df_1} df_1, \quad [10d]$$

In this expression,  $I_{de}$  is associated with the term related to the deformation,  $I_{sh}$  is associated with the

term related to the shrinkage, and  $I_{sh\dot{\epsilon}}$  is associated with the term related to the deformation-induced shrinkage. As can be seen, the second and third terms of Eq. [10a] have the same form, related through the isotherm velocity  $V_T$  and solid deformation velocity  $V_{sx}$ . The permeability  $K$  has also been left inside the integrations of  $I_{de}$ ,  $I_{sh\dot{\epsilon}}$ , and  $I_{sh}$  because many different empirical relations exist for this function,<sup>[21,22]</sup> such as the Kozeny–Carman relation.<sup>[21]</sup>

Following Monroe and Beckerman,<sup>[17]</sup> it is assumed that fluid flow ceases once the pressure drop exceeds  $\Delta P_{cr}$ . Thus, for a given value of  $\Delta P_{cr}$ , the critical fraction of fluid  $f_{lcr}$  can be obtained from Eq. [10]. Further shrinkage and deformation beyond  $f_{lcr}$  will result in the formation of porosity.

When flow stops at  $f_{lcr}$ , mass conservation can be applied to determine the porosity that must form to feed the remaining shrinkage,<sup>[17]</sup>

$$f_{p,sh} = \frac{\beta}{1 + \beta} f_{lcr}. \quad [11]$$

A similar set of variables can be used to calculate deformation-related porosity,  $f_{p,de,ex}$  and  $f_{p,de,ey}$ ,

$$f_{p,de,ex} = \frac{\dot{\epsilon}_{px} \Delta T_f}{\bar{T}} \int_0^{f_{lcr}} (1 - f_l) \frac{d\theta}{df_l} df_l, \quad [12]$$

$$f_{p,de,ey} = \frac{\dot{\epsilon}_{py} \Delta T_f}{\bar{T}} \int_0^{f_{lcr}} (1 - f_l) \frac{d\theta}{df_l} df_l. \quad [13]$$

Finally, because of the term  $I_{sh\dot{\epsilon}}$  in Eq. [10], there is additionally strain rate-induced shrinkage porosity,

$$f_{p,sh\dot{\epsilon}} = \frac{G \dot{\epsilon}_{px} \lambda_2}{\bar{T}} (1 - f_l) = \frac{V_{sx}}{V_T} (1 - f_{lcr}). \quad [14]$$

Thus, as shown in Eqs. [11] through [14], the total porosity that forms during the late stages of solidification below  $f_{lcr}$  consists of four components:  $f_{p,sh}$ ,  $f_{p,de,ex}$ ,  $f_{p,de,ey}$ , and  $f_{p,sh\dot{\epsilon}}$ . Further, the total deformation pore fraction and total pore fraction can be computed and are denoted as  $f_{p,de}$  and  $f_{p,sum}$ , *i.e.*,

$$f_{p,de} = f_{p,de,ex} + f_{p,de,ey}, \quad [15]$$

$$f_{p,sum} = f_{p,sh} + f_{p,sh\dot{\epsilon}} + f_{p,de,ex} + f_{p,de,ey}. \quad [16]$$

Since only a positive strain rate increases pore fraction to result in the formation of a hot tear, the occurrence of a negative strain rate is ignored in the following analysis.

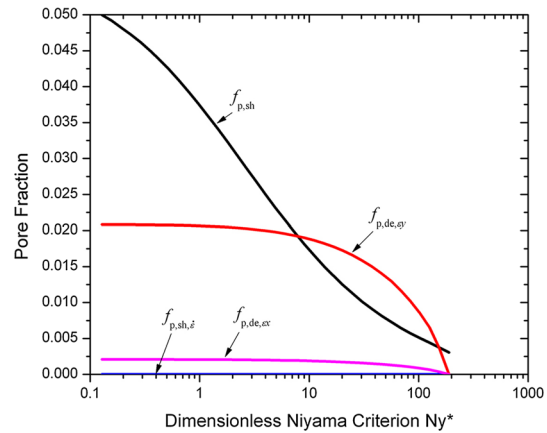


Fig. 2—Pore fraction vs dimensionless Niyama criterion for an Al-3 wt pct Cu alloy with an applied strain rate  $\dot{\epsilon}_{py}$  of  $10^{-3} \text{ s}^{-1}$ .

### B. Effect of Strain Rate Parallel with Thermal Gradient on Pore Fraction

To investigate the predictions of the Pore Fraction hot tearing model and verify its accuracy, the present results are compared against the results provided by Monroe<sup>[17]</sup> for Al-Cu alloys using the same solid fraction–temperature curve and input parameters given in their work (Eq. [17] and Table I in Reference 17). Most importantly,  $\Delta P_{cr}$  is set to 1.0 atm. Note also that the eutectic temperature in Reference 17 should have been given as 821 K (547.85 °C) and not 855 K (581.85 °C) to match the Al-Cu binary phase diagram. To additionally examine the effect of the strain rate parallel with the thermal gradient,  $\dot{\epsilon}_{px}$  is arbitrarily assigned a value of 0.1 times  $\dot{\epsilon}_{py}$ . Figure 2 shows the pore fraction curves as function of  $Ny^*$  for an Al-3 wt pct Cu alloy. The results given in Figure 2 match Figure 3 in Reference 17 but with the addition of the curves  $f_{p,de,ex}$  (Eq. [12]) and  $f_{p,sh\dot{\epsilon}}$  (Eq. [14]). As can be seen, the curves for  $f_{p,sh}$  and  $f_{p,de,ey}$  predict significant porosity, especially at lower values of  $Ny^*$ . For the same  $Ny^*$ , the value of  $f_{p,de,ex}$  is 0.1 times that of  $f_{p,de,ey}$ , as expected. Clearly, the positive value of  $\dot{\epsilon}_{px}$  increases the total deformation pore fraction  $f_{p,de}$ , and  $\dot{\epsilon}_{px}$  has the same impact on the deformation pore fraction as  $\dot{\epsilon}_{py}$  has. The value of  $f_{p,sh\dot{\epsilon}}$  has a magnitude of  $10^{-7}$ , which is negligible compared with the values of  $f_{p,sh}$ ,  $f_{p,de,ey}$ , and  $f_{p,de,ex}$ .

The effect of alloy composition  $C_0$ , thermal gradient  $G$ , and cooling rate  $\bar{T}$  on the pore fraction is shown in Figure 3. The red and black curves in Figure 3 are both calculated with a Niyama criterion (Eq. [1]) value of 100, with the black curves matching those from Figure 5 in Reference 17. The  $f_{p,de,ex}$  curve has the same trend as the  $f_{p,de,ey}$  curve, increasing with composition up to  $C_0 = 0.25$ <sup>[17]</sup> and then decreasing at higher alloy concentrations, identifying the point of maximum hot tearing susceptibility. Thus, the strain rates parallel with and perpendicular to the thermal gradient have the same effect on pore development. As the value of  $f_{p,sh\dot{\epsilon}}$  was negligible, it is not shown in Figure 3. Note that experimentally (*e.g.*,



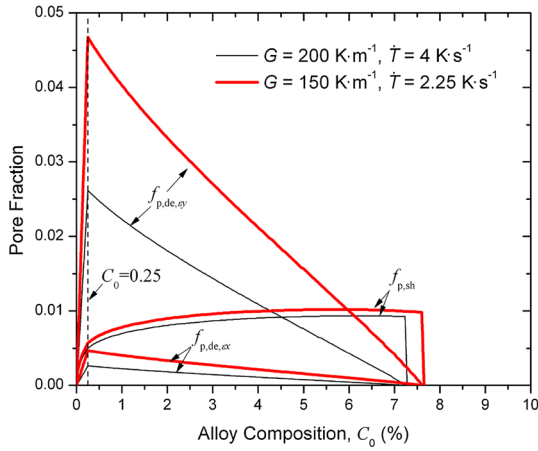


Fig. 3—Pore fraction vs alloy composition for equal Niyama values and an applied strain rate  $\dot{\epsilon}_{py}$  of  $10^{-3} \text{ s}^{-1}$ .

Reference 23), the maximum hot tearing susceptibility for Al-Cu alloys is found at ~Al-1 wt pct Cu alloys and not Al-0.25 wt pct Cu. As explained in detail in Reference 17,  $C_{0,max}$  corresponds to the maximum solidification interval, and it is strongly related to the fraction liquid for grain bridging. In this work, it has been assumed that grain bridging occurs at  $f_l = 0$  in order to compare the results in the present manuscript against Reference 17. An increase in  $f_{l,gb}$  to the usual value of 0.02 ( $f_s = 0.98$ ) will increase  $C_{0,max}$  as well, to 1.36 wt pct Cu.

Surprisingly, by comparing the red and black curves, it can be seen that even with the same Niyama criterion, the pore fractions differ for different cooling rates and thermal gradients. Given the same Niyama criterion, the application of a low cooling rate results in a high pore fraction and thus a high propensity for hot tearing because this results in a decrease in the isotherm speed  $V_T$  (Eq. [3]), which in turn increases the solidification time and finally increases the duration within the brittle temperature region (BTR, *i.e.*, the temperature region within the semi-solid where the ductility of the alloy is virtually zero [24]). [14,25] The effect is much more significant on the deformation-related porosity ( $f_{p,de,ex}$  curve) as compared to the shrinkage-related porosity ( $f_{p,sh}$  curve). This is because the deformation-related porosity is both directly proportional to  $f_{lcr}$  and inversely proportional to  $\dot{T}$ , whereas the shrinkage-related porosity is only proportional to  $f_{lcr}$ . Thus, the Niyama criterion is not sufficient to predict hot tearing susceptibility. Furthermore, although the red and black curves for  $f_{p,sh}$  are similar, identical Niyama values do not indicate identical levels of shrinkage porosity in the context of the present model.

### III. PORE FRACTION PREDICTION FOR DC CASTING UNDER DIFFERENT CONDITIONS

In combination with a finite element simulation, the Pore Fraction hot tearing model can be applied to

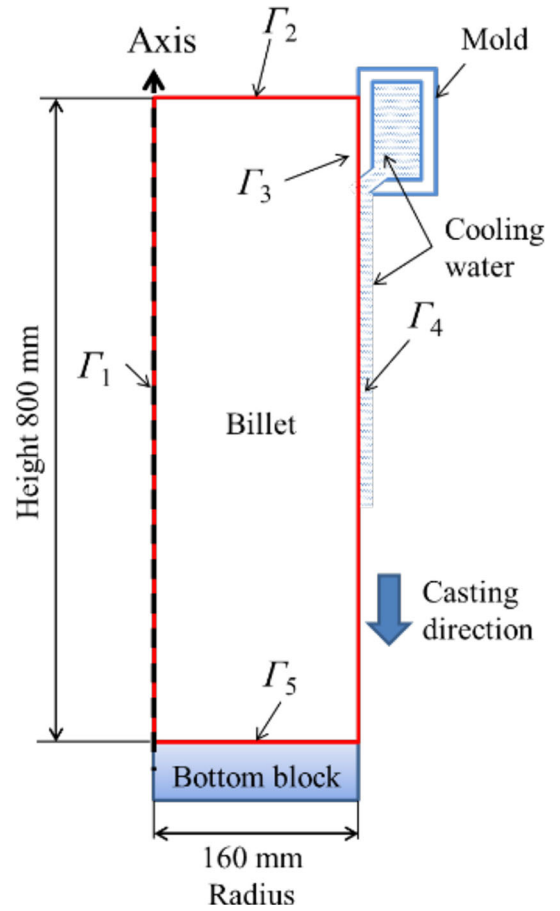


Fig. 4—Schematic of the axi-symmetric DC casting model showing the billet dimensions and placement of the boundary conditions ( $\Gamma_1 - \Gamma_5$ ). [13]

analyze the distribution of  $f_{p,de}$  during DC casting of AA5182 aluminum alloy cylindrical billets.

#### A. Coupled Thermal-Mechanical DC Casting Model

The DC casting process of an AA5182 round billet was simulated using an axi-symmetric coupled thermomechanical model implemented in the commercial FE code Abaqus, which is schematically shown in Figure 4. The details of the simulation methodology, boundary conditions, and constitutive behavior are provided in Jamaly *et al.* [13] The key feature for predicting hot tearing using the Pore Fraction hot tearing model is the alloy's constitutive behavior since this controls the development of the strain rate tensor within the mushy zone. As reported in Reference 13, the modified Ludwik equation developed by Alankar and Wells [26] is used to simulate the constitutive behavior of the alloy at temperatures below the solidus temperature, while the constitutive behavior between the solidus temperature [796.15 K (523 °C)] and the temperature for mechanical coalescence [875.15 K (602 °C)] is simulated based on microstructure and fraction solid according to a model proposed by Phillion *et al.* [27] Above the temperature for mechanical coalescence, a low constant yield strength is specified, matching the yield strength values calculated with the model

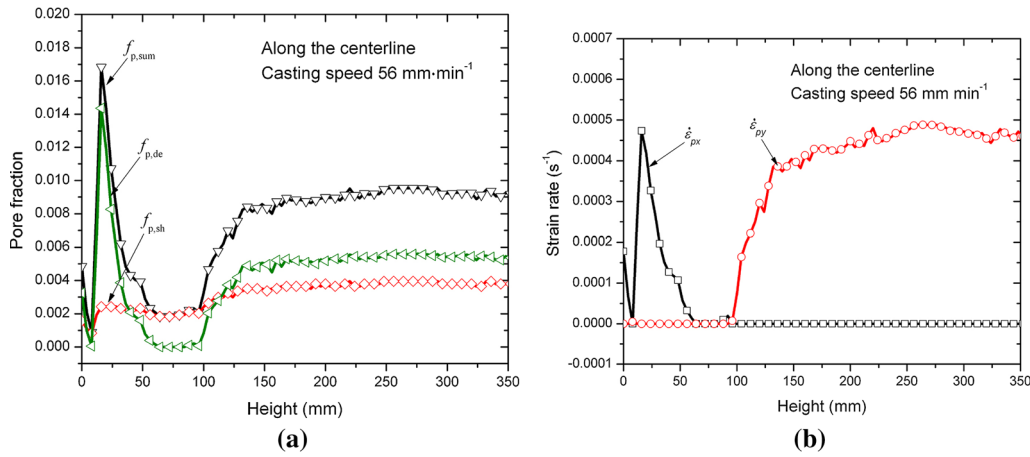


Fig. 5—Distribution of (a) pore fractions vs distance from the bottom block, and (b) strain rate vs distance from the bottom block at a casting speed 56 mm min<sup>-1</sup>.

proposed by Phillion *et al.*<sup>[27]</sup> at the temperature for mechanical coalescence.

### B. Implementation of Pore Prediction Model

The pore fractions were calculated using a C# purpose-written code. First, the DC casting finite element simulation of Jamaly *et al.*<sup>[13]</sup> was run to completion. Second, the cooling rate, thermal gradient, and strain rate was extracted from the simulation output at the critical temperature of 819.15 K (546 °C), corresponding to a solid fraction of 0.98. Third, all the negative strain rate values were set to zero because they do not increase the pore fraction. Finally, the Pore Fraction hot tearing model was applied to calculate  $f_{p,sh}$ ,  $f_{p,de,xy}$ ,  $f_{p,de,ex}$ , and  $f_{p,sh}$ .

The computation of permeability *via* the Kozeny–Carman equation requires the secondary dendrite arm spacing  $\lambda_2$  (SDAS). Following Glenn *et al.*,<sup>[28]</sup> SDAS is calculated as

$$\ln(\lambda_2) = 0.47 \ln(\tau_f) + 1.75, \quad [17]$$

where the unit of  $\lambda_2$  is  $\mu\text{m}$  and  $\tau_f$  is the local solidification time (s) defined as the duration between the liquidus [910.15 K (637 °C)] and solidus [796.15 K (523 °C)] temperatures.

The computation of the strain rates parallel with and perpendicular to the fluid flow within the mushy zone requires a rotation of the strain rate tensor from the global axi-symmetric coordinate system to the local system aligned with the thermal gradient. The strain rate is calculated as follows:

$$A = R \times \dot{\epsilon}_{ij} \times R', \quad [18a]$$

$$R = \begin{bmatrix} \cos(\frac{\pi}{2} - \gamma) & \sin(\frac{\pi}{2} - \gamma) \\ -\sin(\frac{\pi}{2} - \gamma) & \cos(\frac{\pi}{2} - \gamma) \end{bmatrix}, \quad [18b]$$

where  $\gamma$  is the rotation angle between the radius and the thermal gradient,  $R$  is the transformation matrix,  $\dot{\epsilon}_{ij}$  is the strain rate tensor in the global coordinates, and  $A$  is

the strain rate in the local coordinates. The strain rate perpendicular to the thermal gradient,  $\dot{\epsilon}_{py}$ , is given by  $A_{11} + \dot{\epsilon}_{pH}$  where  $\dot{\epsilon}_{pH}$  is hoop plastic strain rate, and the strain rate parallel to the thermal gradient,  $\dot{\epsilon}_{px}$ , is  $A_{22}$ .

### C. Effect of Strain Rate Parallel with Thermal Gradient on Pore Fraction

Figure 5 shows (a) the pore fraction distribution along the centerline of the billet at a casting speed of 56 mm min<sup>-1</sup>, and (b) the corresponding strain rates parallel with and perpendicular to the thermal gradient. Figure 5(a) shows that the part of the billet at 16 mm from the bottom of the billet has the highest pore fractions  $f_{p,de}$  and  $f_{p,sum}$ , which make this region prone to hot tearing. The total deformation pore fraction  $f_{p,de}$  then undergoes a steep decrease as the height increases from 16 mm, and  $f_{p,de}$  is less than  $10^{-4}$  at 48 mm from the bottom of the billet. After a distance of 96 mm from the bottom of the billet,  $f_{p,de}$  starts to increase again as the strain rate  $\dot{\epsilon}_{py}$  acquires a tensile nature (as shown in Figure 5(b)) and finally reaches a plateau. Note that each height value is a multiple of four since that is the mesh size in the finite element simulation. Although the maximum value of  $\dot{\epsilon}_{py}$  is similar to the maximum value of  $\dot{\epsilon}_{px}$ , the pore fraction in the steady-state regime above 96 mm is significantly smaller than that at 16 mm because of the different thermal conditions. In the start-up regime, the cooling rate and thermal gradient are very low (although the Niyama value is larger than the steady state) because the contact heat transfer coefficient between the billet and the bottom block is considerably lower than the water film heat transfer coefficient.

The importance of including the strain rate parallel to the thermal gradient is evident in Figure 5(b), since all of the tensile deformation occurring in the start-up region is in this direction, while  $\dot{\epsilon}_{py}$  remains at zero until a distance of 96 mm from the bottom of the billet. Without including  $\dot{\epsilon}_{px}$ , the deformation pore fraction would be very small within a distance of 96 mm from bottom of the billet, making it appear that the shrinkage

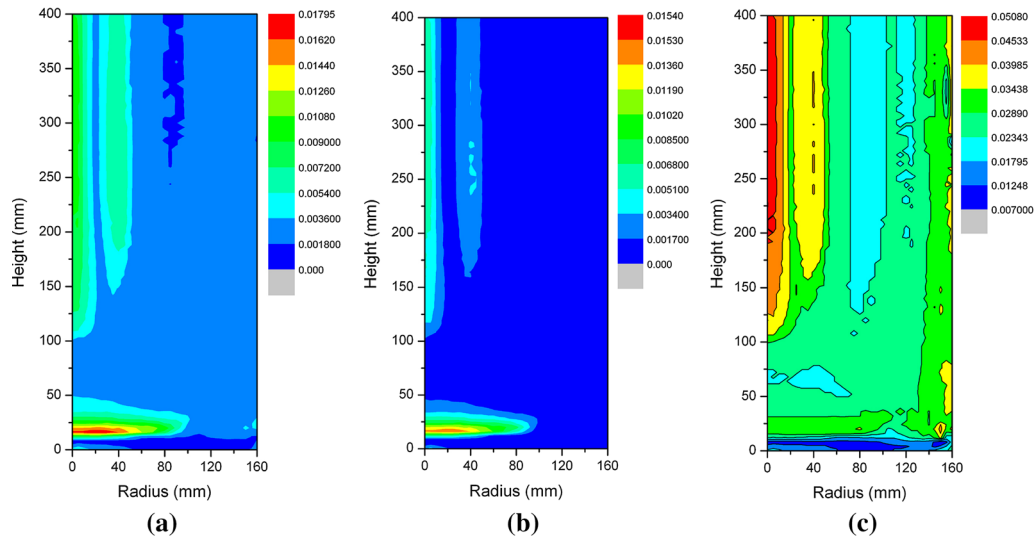


Fig. 6—Contour maps showing the variation of pore fractions (a)  $f_{p,sum}$ , (b)  $f_{p,de}$ , and critical liquid fraction (c)  $f_{lcr}$  throughout the billet for a casting speed of  $56 \text{ mm min}^{-1}$ .

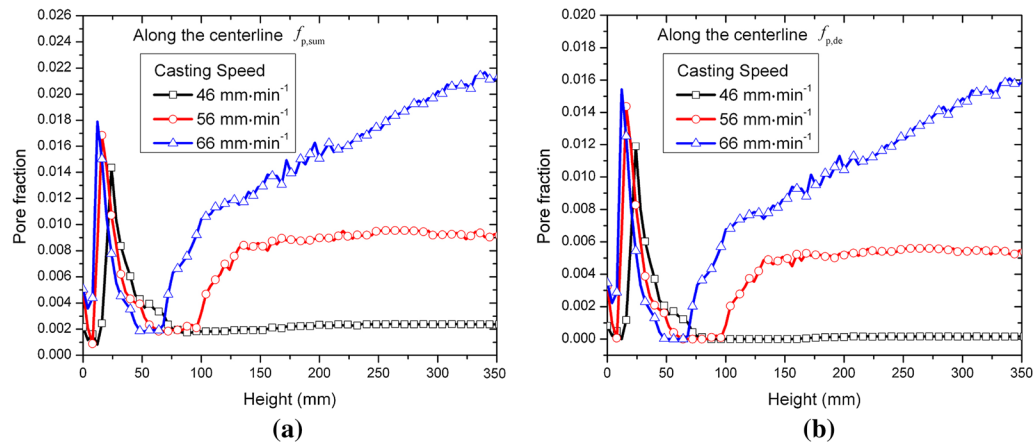


Fig. 7—Distribution of pore fractions (a)  $f_{p,sum}$  and (b)  $f_{p,de}$  along the centerline of the billet at different casting speeds.

pore fraction dominates within this region. This would lead to erroneous conclusions regarding the relative importance of the shrinkage and deformation pore fractions as predictors for hot tearing formation within the start-up region of DC casting. Furthermore, this would lead to the appearance that the total pore fraction increases with increasing distance from bottom of the billet, *i.e.*, hot tearing susceptibility is increased in the steady-state region as compared to the start-up region. This would not match industrial experience.

Figure 6 shows the contour plots of the pore fractions  $f_{p,de}$  and  $f_{p,sum}$  and the critical liquid fraction  $f_{lcr}$  using the casting conditions corresponding to Figure 5. The highest values of the pore fractions  $f_{p,de}$  and  $f_{p,sum}$  appear at a radius of 15 mm and a distance of 16 mm from bottom of the billet. The part at which  $f_{p,de}$  exceeds  $10^{-2}$  is concentrated in a small region, between 12 and 26 mm above the bottom block and within 70 mm on the centerline. This region is within the start-up phase of DC casting. Thus, if hot tears are to occur, they should

appear within this region. Large values of  $f_{p,de}$  equate to a high susceptibility to hot tearing due to their link with tensile strain. Examining Figure 6(c), it can be seen that the highest  $f_{lcr}$ , *i.e.*, the fraction of liquid at which feeding ceases to occur, is found much further up the casting, within the steady-state region, and has a value of  $f_l = 0.95$ . However, the highest  $f_{lcr}$  does not correspond with the highest  $f_{p,de}$  and  $f_{p,sum}$  because of the strong dependence of these terms on thermal gradient, cooling rate, and strain rate.

#### D. Effect of Casting Speed

Figure 7 shows the effect of casting speed on (a) total pore fraction  $f_{p,sum}$  and (b) total deformation pore fraction  $f_{p,de}$  along the centerline of the billet. Both figures show the maximum values of pore fraction as well as the hot tearing sensitivity increase with increasing casting speed. Similar results were obtained by Drezet and Rappaz;<sup>[29]</sup> that is, in the DC casting

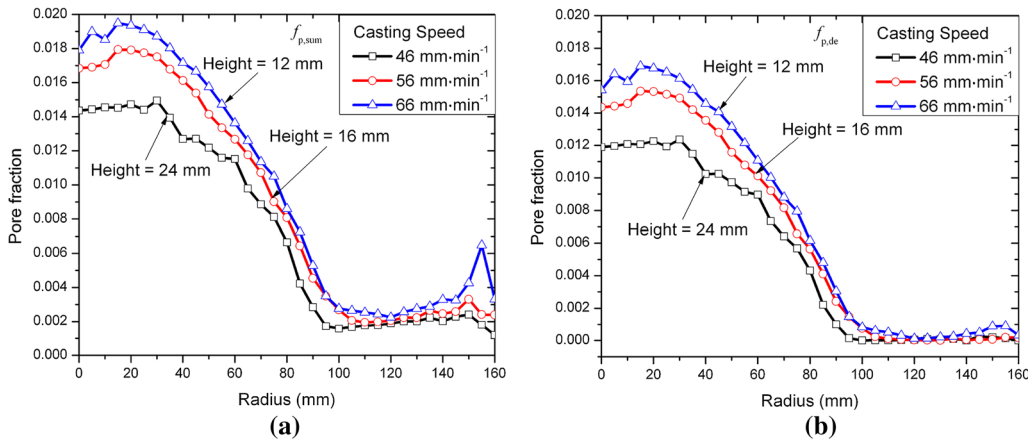


Fig. 8—Distribution of pore fractions (a)  $f_{p,sum}$  and (b)  $f_{p,de}$  along the radius of the billet at different casting speeds.

process, a high casting speed results in large pressure drops and high hot tearing tendencies according to the RDG criterion. However, Figure 7 also shows that the location of the maximum point of the pore fraction moves downward along the centerline as the casting speed increases. This phenomenon indicates that a high casting speed equates to a high hot tearing tendency, but hot tearing in this case occurs early after the start of DC casting. Beyond a distance of 50 mm from the bottom of the billet, the deformation pore fraction rapidly increases again in cases in which the casting speeds are 56 and 66 mm min<sup>-1</sup>. This condition is due to the increase in the strain rate  $\dot{\epsilon}_{py}$ , as shown in Figure 5(b). In contrast, nearly no increase in the deformation pore fraction occurs when the casting speed is 46 mm min<sup>-1</sup>.

In the start-up region of the casting, the maximum pore fractions are observed at 24, 16, and 12 mm from the bottom for the casting speeds of 46, 56, and 66 mm min<sup>-1</sup>, respectively. Figure 8 shows the curves of  $f_{p,de}$  and  $f_{p,sum}$  along the radius and crossing the maximum points at different casting speeds. Similar to the trend shown in Figure 7, the increase in casting speed raises the pore fraction and finally raises the hot tearing probability. The regions where  $f_{p,de}$  exceeds 10<sup>-3</sup> are mainly within the radius range of 0 mm to 100 mm. Hence, the central part of the billet is sensitive to hot tearing.

#### E. Comparison with Prior Models

Based on RDG criterion, Drezet *et al.*<sup>[29]</sup> concluded that during the DC casting, the bottom of the billet is more sensitive to hot tearing than the region of the primary cooling, and the process conditions used to start the casting are critical. Hao *et al.*<sup>[30]</sup> investigated hot tearing during DC casting of AZ31 magnesium billet, showing that the locations near the base of the ingot are more sensitive to hot tearing, and that faster casting speeds tend to exacerbate hot tear formation. Thus, the results given in this work that include a term accounting for the strain rate parallel to the thermal gradient match qualitatively the previous findings. However, as shown in Figure 5, without including the

term  $\dot{\epsilon}_{px}$ , hot tearing susceptibility is predicted to be enhanced in the start-up region because of the shrinkage term and not because of the strain rate term. Ideally, a criterion for predicting hot tearing would show greater dependence on the amount of deformation as compared to porosity developing within the semi-solid. In work on steels, Monroe and Beckermann<sup>[31]</sup> developed a hot tearing indicator in which hot tearing susceptibility was determined based on the integral of the volumetric strain rate after liquid feeding has ceased. In that work, shrinkage-based and deformation-based porosity were only loosely coupled, whereas in our model, the shrinkage and deformation terms are fully integrated. Thus, the Pore Fraction hot tearing model proposed in this work represents the continued and natural evolution of the RDG criterion toward ultimately quantitatively predicting the occurrence of hot tears.

## IV. CONCLUSIONS

The strain rate parallel with the thermal gradient has been added to a pressure drop equation in the mushy zone that already includes the effects of strain rate perpendicular to the thermal gradient and shrinkage feeding in order to improve hot tearing predictions based on the dimensionless Niyama criterion. Application of this criterion to analytical simulations of the casting of an Al-3 wt pct Cu alloy, and FE simulations of the DC casting process for the aluminum alloy AA5182 has demonstrated the following:

- (a) For the casting simulation of Al-3 wt pct Cu alloy, under the same Niyama criterion, a decrease in the cooling rate increases significantly the deformation pore fraction and increases moderately the shrinkage pore fraction. Thus, the Niyama criterion is insufficient as a predictor for hot tear formation.
- (b) For the DC casting simulation and hot tearing prediction of AA5182 alloy,
  - Including the strain rate parallel to the thermal gradient strongly improves the predictive



quality of hot tearing criteria based on a pressure drop equation. Without this term, the deformation pore fraction would be very small in the start-up region of DC casting as compared to the shrinkage pore fraction, and the total pore fraction would be highest in the steady-state region.

- An increase in casting speed increases both the deformation and shrinkage pore fractions, resulting in an increase in the probability of hot tearing. An increase in casting speed also causes the location of highest hot tearing susceptibility to move toward the bottom part of the billet.

#### ACKNOWLEDGMENT

This work was funded by the China Scholarship Council, and the National Science and Engineering Research Council of Canada.

#### REFERENCES

1. J. Campbell: *Castings*, 2nd ed., Butterworth-Heinemann, Oxford, 2003.
2. J. Drezet, M. Rappaz, and Y. Krahenbuhl: *Mater. Sci. Forum*, 1996, vols. 217–222, pp. 305–10.
3. D.G. Eskin, M. Lalpoor, L. Katgerman: Published in *TMS-Light Metals*, S.J. Lindsay, ed., TMS, Warrendale, PA, 2011, pp. 669–74.
4. B. Commet, P. Delaire, J. Rabenberg, et al.: Published in *TMS-Light Metals*, P.N. Crepeau, ed., TMS, Warrendale, PA, 2003, pp. 711–17.
5. M. Lalpoor, D.G. Eskin *et al.*: *Mater. Sci. Eng. A*, 2011, vol. 528, pp. 2831–42.
6. J. Grandfeld and P. McGlade: *Mater. Sci. Forum.*, 1996, vol. 20, pp. 29–51.
7. D.G. Eskin, Q. Du, and L. Katgerman: *Metall. Mater. Trans. A*, 2008, vol. 39A, pp. 1206–12.
8. D.G. Eskin and L. Katgerman: *Mater. Technol.*, 2009, vol. 24, pp. 152–56.
9. K.D. Carlson and C. Beckermann: *Metall. Mater. Trans. A*, 2009, vol. 40A, pp. 163–75.
10. J.A. Dantzig and M. Rappaz: *Solidification*, 1st ed., EPFL Press, Lausanne, 2009.
11. I. Farup, J.M. Drezet, and M. Rappaz: *Acta Mater.*, 2001, vol. 49, pp. 1261–69.
12. A.B. Phillion, S.L. Cockcroft, and P.D. Lee: *Mater. Sci. Eng. A*, 2008, vol. 491, pp. 237–47.
13. N. Jamaly, A.B. Phillion, and J.M. Drezet: *Metall. Mater. Trans. B*, 2013, vol. 44B, pp. 1287–95.
14. Y. Won, T. Yeo, D. Seol *et al.*: *Metall. Mater. Trans. B*, 2000, vol. 31B, pp. 779–94.
15. M. Rappaz, J.-M. Drezet, and M. Gremaud: *Metall. Mater. Trans. A*, 1999, vol. 30A, pp. 449–55.
16. T. Clyne and G. Davies: *Br. Foundrym.*, 1981, vol. 74, pp. 65–73.
17. C. Monroe and C. Beckermann: *JOM*, 2014, vol. 66, pp. 1439–45.
18. E. Niyama, T. Uchida, M. Morikawa, and S. Saito: *AFS Cast Met. Res. J.*, 1982, vol. 7, pp. 52–63.
19. J. Sengupta, S.L. Cockcroft *et al.*: *Mater. Sci. Eng. A*, 2005, vol. 397, pp. 157–77.
20. J.-M. Drezet and M. Rappaz: *Metall. Mater. Trans. A*, 1996, vol. 27A, pp. 3214–25.
21. A.W.H. Heijs and C. Lowe: *Phys. Rev. E*, 1995, vol. 51, pp. 4346–52.
22. S. Ergun: *Chem. Eng. Prog.*, 1952, vol. 48, pp. 89–94.
23. D.G. Eskin and L. Katgerman: *Prog. Mater. Sci.*, 2004, vol. 49, pp. 629–711.
24. B. Magnin, L. Maenner *et al.*: *Mater. Sci. Forum*, 1996, vols. 217–222, pp. 1209–14.
25. A. Yamanaka, K. Nakajima, *et al.*: *Revue Metall.-Cahiers D Inf. Techn.*, 1992, vol. 89, pp. 627–33.
26. A. Alankar and M.A. Wells: *Mater. Sci. Eng. A*, 2010, vol. 527, pp. 7812–20.
27. A.B. Phillion, S.L. Cockcroft, and P.D. Lee: *Model. Simul. Mater. Sci. Eng.*, 2009, vol. 17, pp. 1–15.
28. A.M. Glenn, S.P. Russo, and P.J.K. Paterson: *Metall. Mater. Trans. A*, 2003, vol. 34A, pp. 1513–23.
29. J.M. Drezet and M. Rappaz: *TMS-Light Metals*, J.L. Angier, ed., TMS, Warrendale, PA, 2001, pp. 887–93.
30. H. Hao, D.M. Maijer *et al.*: *Metall. Mater. Trans. A*, 2010, vol. 41A, pp. 2067–77.
31. C. Monroe and C. Beckermann: *Mater. Sci. Eng. A*, 2005, vols. 413–414, pp. 30–36.